AEROSPACE REPORT NO.
TOR-2020-01948

Redesign of the Particle-Impact Shock Tube and Preliminary Data Analysis

July 29, 2020

Joshua D. Winner[1] and James H. Morehart[2]
[1]Chemical Propulsion and Environmental Science, Propulsion Science Department
[2]Launch, Strike and Range, Developmental Prototypes and Projects

Prepared for:

Space and Missile Systems Center
Air Force Space Command
483 N. Aviation Blvd.
El Segundo, CA 90245-2808

Contract No. FA8802-19-C-0001

Authorized by: Space Systems Group

Abstract

The particle-impact shock tube (PST) located at The Aerospace Corporation provides a test environment to investigate the ignition resistance of metals in high-pressure, oxygen-rich conditions. It is important to characterize candidate alloys intended for use in rocket engines for their ignition resistance. The PST has recently undergone rebuilding and modifications, namely with a new expansion region and test section made entirely of hardened Monel K500, and the addition of a copper liner in the test section. This redesign provides improvements to both the safety of the experiment, as well as allowing its operation with higher oxygen fill pressures than previously permitted (fill pressures above 2000 psi are now accessible). This report discusses the circumstances that led to the rebuild, the details of the redesign, and a preliminary look at the performance of the PST with the new expansion region and test section.

Contents

1. Introduction and Background 1
2. Modifications to Particle Shock Tube 8
3. Performance and Results 11
4. Conclusions 14
5. Acronyms 15
6. References 16

Figures

Figure 1. A diagram of the PST experimental setup. 1
Figure 2. Images of the ruptured expansion section of the particle shock tube. 2
Figure 3. An image of the interior of the expansion region of the PST. Significant metal deposits are present within the cell. The red circle denotes one such area of deposits that formed on a sharp feature of the interior of the cell, where local heating is expected to be higher than the 100° C predicted via conduction. 3
Figure 4. The sampling location of the metal deposit which was found to contain ~10% elemental titanium. 3
Figure 5. EDS results from the sampled region in Figure 4, showing a relatively high (~10%) concentration of titanium in the sampling area. On the left is an electron image and the right image shows a false- color mapping of the same image with elemental titanium highlighted. 4
Figure 6. The top right image shows the location of the sampled o-ring segment, the top left image shows an electron image of a tear in the o-ring, which was tested with EDS. The high concentration of magnesium on the surface of the o-ring is a result of the high rate of absorption of Viton o-rings with metal particles.[3] 5
Figure 7. A graph of the onset of exothermic combustion in Viton with increasing magnesium density.[3] 6
Figure 8. An image of a machining defect on the window arm of the expansion cell. 6
Figure 9. An image of the three o-ring design of the window arm, with several design flaws labelled. 7
Figure 10. Diagrams of the new expansion region as well as the Cu liners and attached antechamber. Several novel safety features are labelled, as well as the new positioning of the particle loading ports. 8
Figure 11. A graph showing the predicted venting times of the expansion chamber with both the old diameter venting lines (red circles) and the new larger diameter venting lines (black triangles). 9
Figure 12. A model of the three sacrificial copper fittings in the new expansion chamber design. The lower image shows a closeup of the copper nozzle insert. 10
Figure 13. Images from the FEM analysis predictions of the new expansion section. 11
Figure 14. Pressure trace from the new PST expansion cell. The driven section pressure was 700 psi and the driver region burst pressure was 30 ksi. Several shock reflections are observed after the initial shock wave impact. 12
Figure 15. The pressure trace shown in Figure 14 converted to frequency space. A clear peak is visible at 1812 Hz. 13

1. Introduction and Background

The particle-impact shock tube (PST), built by The Aerospace Corporation, was designed to investigate the ignition resistance of metal alloys due to collisions of particles in a high-pressure, oxygen-rich environment. This specialized testing is useful in the evaluation of candidate metal alloys for use in high-risk areas of rocket engines. Most recently, the PST was used to conduct a series of tests on additively manufactured (AM) material samples. Additive manufacturing provides the advantages of short production lead times and design flexibility typically unavailable with conventional machining [1]. Several rocket engine manufacturers have already brought AM components into service. However, the susceptibility of AM materials and even conventional superalloys to particle-impact ignition in more stressing environments, such as those in oxidizer-rich staged combustion or full-flow staged combustion engines, remains a critical feature of testing as AM popularity increases. In this regard, the PST is a tool that provides a means to test the ignition susceptibility due to particle impact of virtually any metal alloy in high-pressure, oxygen-rich conditions [2].

The PST has three distinct regions; a driver gas section, a driven gas section, and an expansion region. These are depicted notionally below in Figure 1. Initially, the driven gas section is pressurized, typically with oxygen up to 2000 psi. Following this pressurization, a metal target mounted in the test section is heated to approximately 500 degrees C. These conditions approach the environment within a staged-combustion rocket engine. Following sample heating, the driver section, which is separated by a burst disc, is pressurized with helium "driver gas" to a pressure of 10,000 to 60,000 psi. Once the driver gas reaches a critical pressure, the disc ruptures and creates a shock wave that propagates down the driven section of the shock tube. The oxygen "driven gas" is accelerated behind this shock. Further downstream in the driven section, aluminum particles are entrained in the flow behind the shock wave and are carried until impacting the metal target.

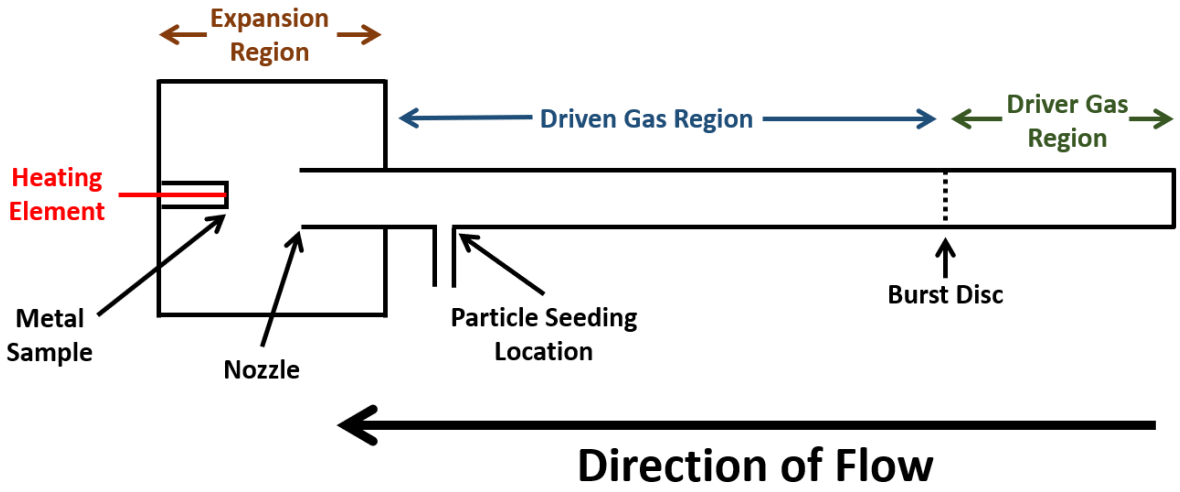

Figure 1. A diagram of the PST experimental setup.

Since the driven section is pressurized with oxygen, this setup mimics real-world staged-combustion engines where particle impact ignition events can occur.[2] During normal operation of the PST, a high-pressure rupture occurred in the expansion region. This rapid unplanned depressurization included the combustion of portions of the 17-4 stainless steel expansion region. Images of this rupture can be seen in Figure 2. This rupture led to a large shockwave in the immediate area of the experiment as the high-pressure oxygen was rapidly vented to the open atmosphere.

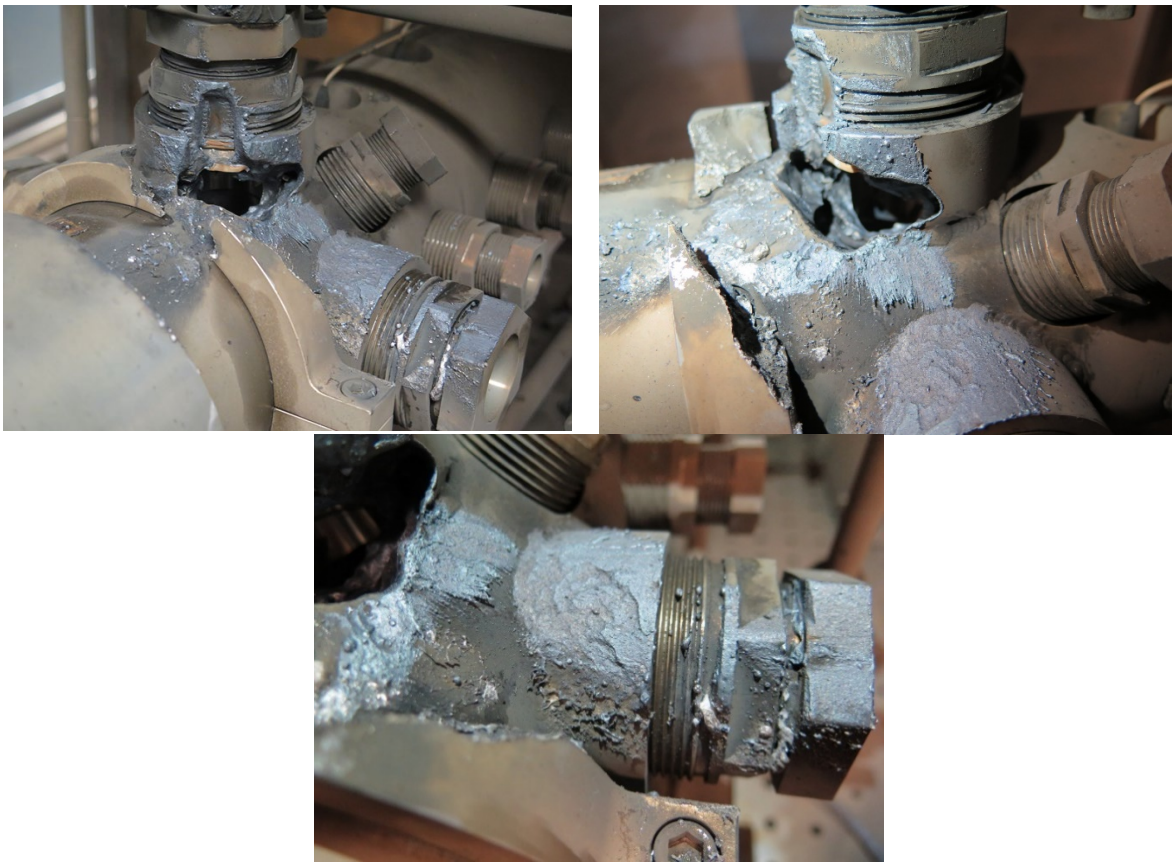

Figure 2. Images of the ruptured expansion section of the particle shock tube.

This rupture had several possible causes. Most likely, a kindling chain event occurred, resulting in the ignition of the interior walls of the expansion section. Metal test samples in this region are typically heated to 500 degrees C. This creates a temperature gradient within the expansion region between the metal sample and the chamber walls. However, an estimate of the conduction heat transfer only predicts an interior wall temperature of ~100 degrees C. Conduction is the dominant mechanism of heat transfer for this system, with radiative heat transfer playing a relatively small role. The predicted heating could be significantly larger at sharp edges within the chamber. Therefore, this rupture is believed to be the result of the ignition of a contaminant, since these temperatures are too low to cause the failure of stainless steel as seen in this incident. Viton O-rings were present in the window mounting locations of the expansion region and are known to have a relatively low temperature of combustion [3]. Another possible source of ignition was metal deposits, which built up on the interior of the expansion region due to prior runs where either aluminum particle combustion or metal target combustion occurred. Evidence of such metal deposits can be seen highlighted in Figure 3.

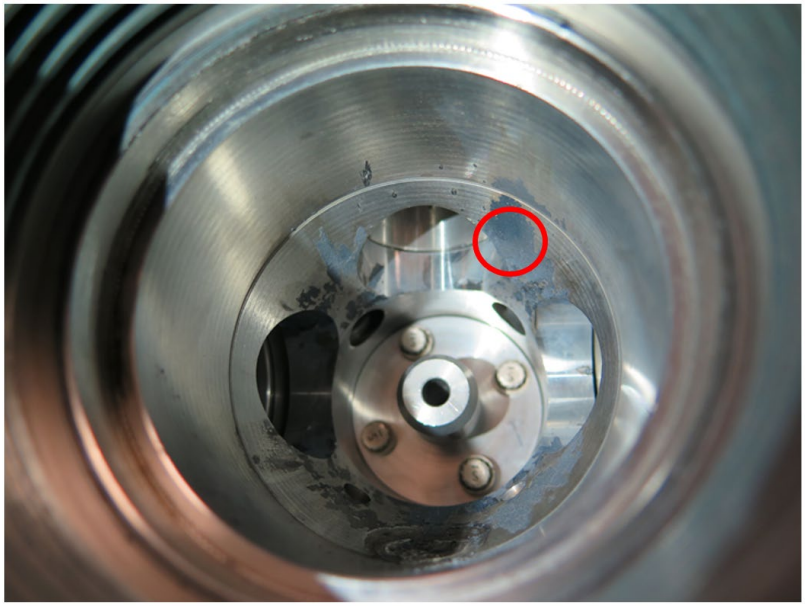

Figure 3. An image of the interior of the expansion region of the PST. Significant metal deposits are present within the cell. The red circle denotes one such area of deposits that formed on a sharp feature of the interior of the cell, where local heating is expected to be higher than the 100° C predicted via conduction.

The expansion region was sectioned via wire electrical discharge machining (EDM), to assess any inherent design flaws. Also, metal deposits at several locations within the expansion region were sampled and tested with energy dispersive X-ray spectroscopy (EDS), which measures the spatially resolved elemental composition of the deposit [4][5]. One area near the apparent rupture site (see Figure 4) was found to contain a high concentration of titanium, as shown in Figure 5. These deposits are believed to be the direct result of previous testing in the PST involving titanium metal targets, which experienced a significant amount of combustion due to aluminum particle impacts. It is unclear if the titanium residue is fully oxidized.

Figure 4. The sampling location of the metal deposit which was found to contain ~10% elemental titanium.

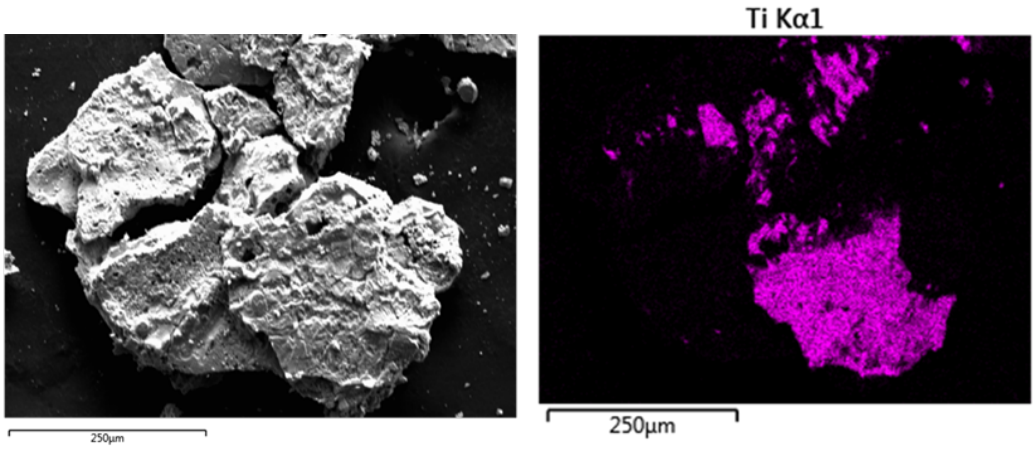

Figure 5. EDS results from the sampled region in Figure 4, showing a relatively high (~10%) concentration of titanium in the sampling area. On the left is an electron image and the right image shows a false-color mapping of the same image with elemental titanium highlighted.

Another possible source of ignition was magnesium detected on Viton remnants in the immediate vicinity of the rupture. EDS measurements were performed on a sample of the remaining o-ring and a high concentration of magnesium was found to be present. These EDS results can be seen below in Figure 6. Metal particulates dispersed in Viton have been reported to undergo exothermic decomposition at even slightly elevated temperatures.[3] For magnesium, these ignition temperatures have been measured as low as 106 degrees C, with a strong dependence on concentration as shown in Figure 7. This magnesium could have been present from either previously tested magnesium targets (more probable) or it may be a result of dust settling on the exposed o-rings from the partial combustion of the holding stands used on the exterior of the PST, which contained some amount of magnesium.

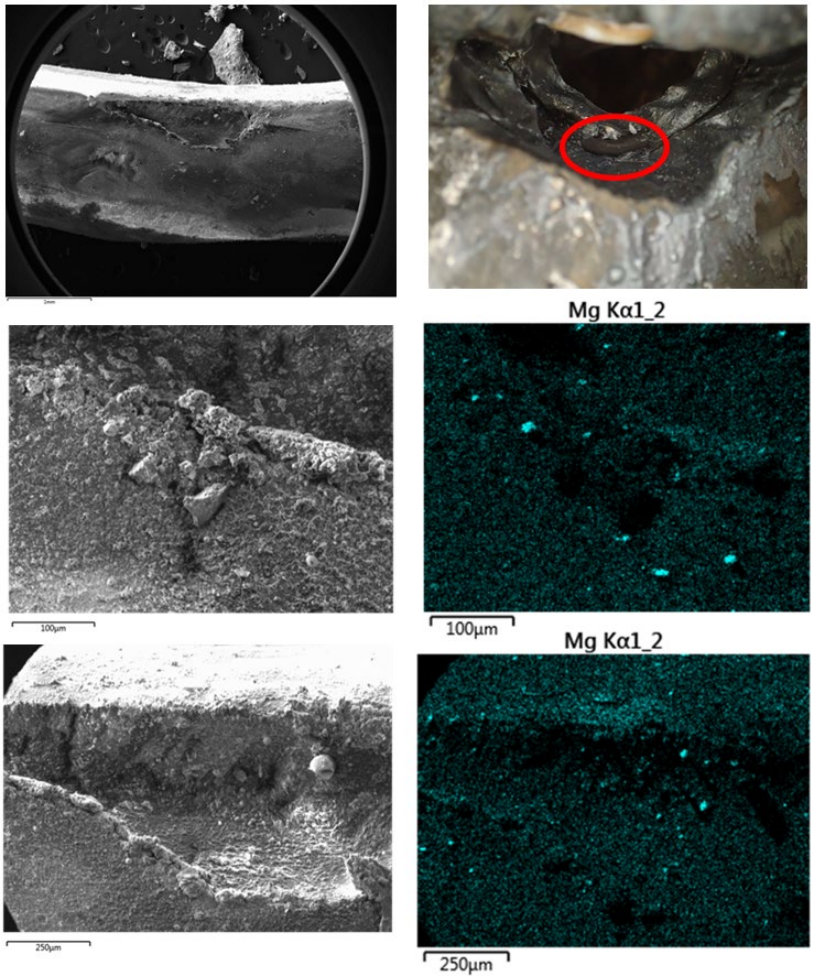

Figure 6. The top right image shows the location of the sampled o-ring segment, the top left image shows an electron image of a tear in the o-ring, which was tested with EDS. The high concentration of magnesium on the surface of the o-ring is a result of the high rate of absorption of Viton o-rings with metal particles.[3]

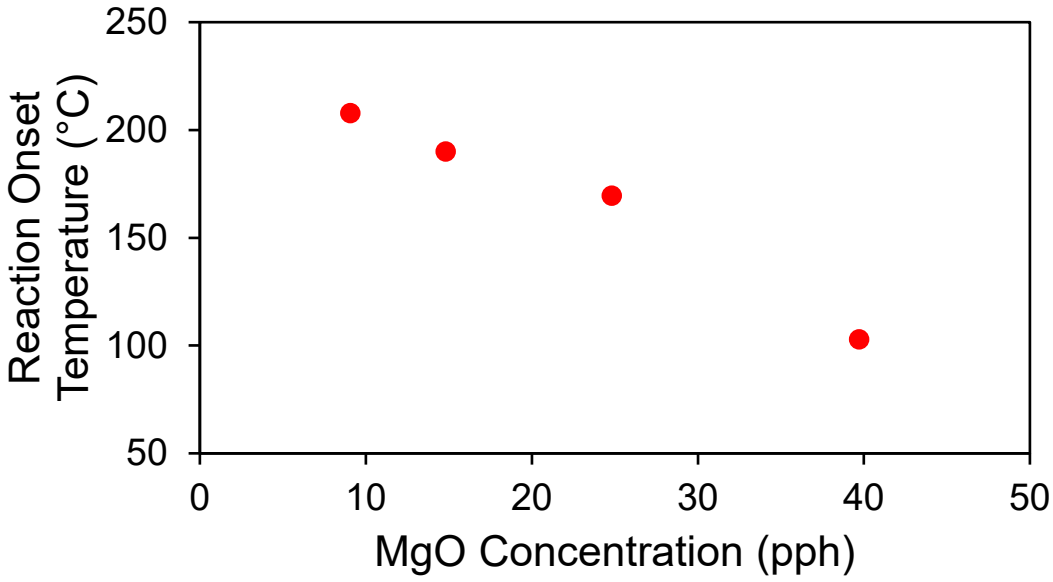

Figure 7. A graph of the onset of exothermic combustion in Viton with increasing magnesium density.[3]

Since the rupture event occurred adjacent to the window mounting arm of the expansion cell, it is postulated that the window assembly may contain inherent flaws. The window mounting assembly utilizes three separate o-ring seals. However, after sectioning the expansion cell, machining defects were discovered which allowed gas in the expansion cell to completely bypass the first o-ring seal. This can be seen below in Figure 8. The machining defect is denoted with a red arrow, where the machining of the section bypassed the first window assembly o-ring, located flush on the bottom of the window mount.

Figure 8. An image of a machining defect on the window arm of the expansion cell.

The arrangement of the three o-ring seals in the window arm is shown *vide infra*. Several aspects of the design are of note. The third o-ring is located next to a right-angle opening, which would lead to an increased rate of degradation of the o-ring due to expansion and contraction resulting from pressure cycling. A large cavity is also present beyond the third o-ring seal, which runs around the entire diameter of the window arm. A rapid expansion of high-pressure oxygen into this cavity could potentially result in significant frictional heating, which could then cause an ignition event. This cavity also appears to be the

central point where the rupture originated from in the expansion cell. Lastly, it should be noted that the overall weld penetration for the window arm is relatively low. This could lead to a high-pressure failure, if the o-ring setup were to fail as well.

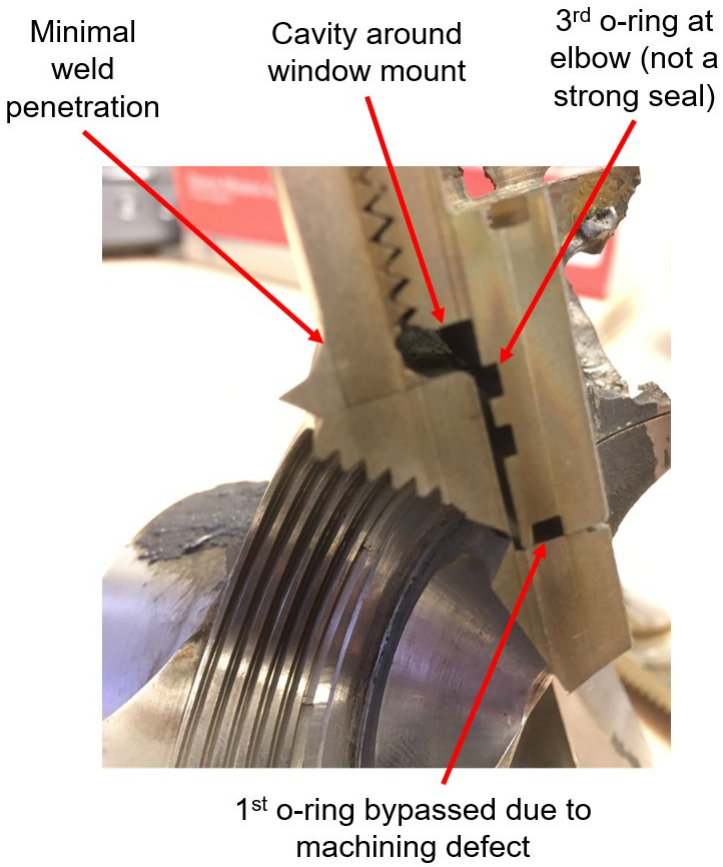

Figure 9. An image of the three o-ring design of the window arm, with several design flaws labelled.

Because of these potential failure modes, a significant redesign effort was undertaken for the PST, with a focus on increased safety following target ignition events. This report presents the new design features incorporated into the PST expansion region, the mitigation steps taken since the rupture incident, and the initial testing and results using this new expansion region. These developments improve the safety of particle impact experiments, and allow higher pressure oxygen conditions, both of which are desired for more relevant testing.

2. Modifications to Particle Shock Tube

The new expansion region of the PST has been designed to mitigate risks from extensive target combustion as well as provide a testing environment for high pressure gaseous oxygen studies (>2000 psi). This cell has been designed to mitigate any future kindling chain events resulting from either aluminum particle combustion, target metal combustion, or a combination of the two. The overall design of the cell also eliminates all the potential failure modes discussed previously in this work.

The new expansion region is made entirely of Monel K500 hardened stock. This stands as an improvement over the previous design, which was constructed of 17-4 stainless steel, which is far more susceptible to combustion events. Monel K500 has been tested in the past to be safe for usage in high pressure (10,000 psi), high temperature (500 degrees C) oxygen systems [6][7].

In addition to manufacturing the new expansion region out of Monel K500, this chamber has twice the wall thickness of the previous expansion cell. The higher wall thickness allows for weldless window inserts on the new cell. As previously seen in Figure 8, the welds of the previous expansion chamber were considered a weak point and potential source of failure. The new weldless design can be seen below in Figure 10. Also, of note is the new location of particle loading ports. Placing these ports closer to the nozzle exit leads to a lower chance of particle impacts along the interior of the shock tube. This also results in particle impacts on test samples at higher pressures, since particle arrival times are reduced significantly following the shock wave. Another new feature is the increased diameter of the post-experiment venting lines. In the previous expansion cell design, ¼" Hi-P fittings were used for venting the chamber post-shock. This led to venting times on the order of 10s of seconds. With the new wider diameter, flow conductance is increased and vent out times are expected to be on the order of one-tenth of a second [8]. This is beneficial in the case of emergency venting, where rapid depressurization of oxygen may be required to quench a sustained ignition event. A graph showing the predicted venting speeds, with an initial pressure of 2000 psi can be seen in Figure 11.

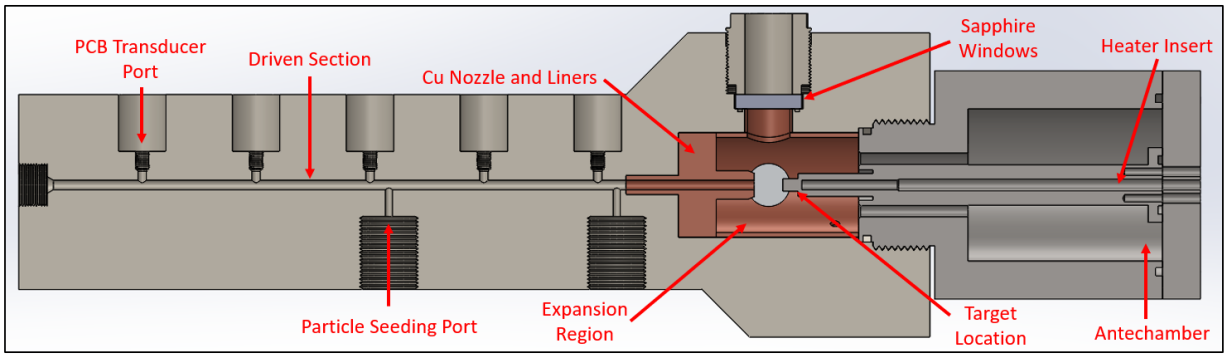

Figure 10. Diagrams of the new expansion region as well as the Cu liners and attached antechamber. Several novel safety features are labelled, as well as the new positioning of the particle loading ports.

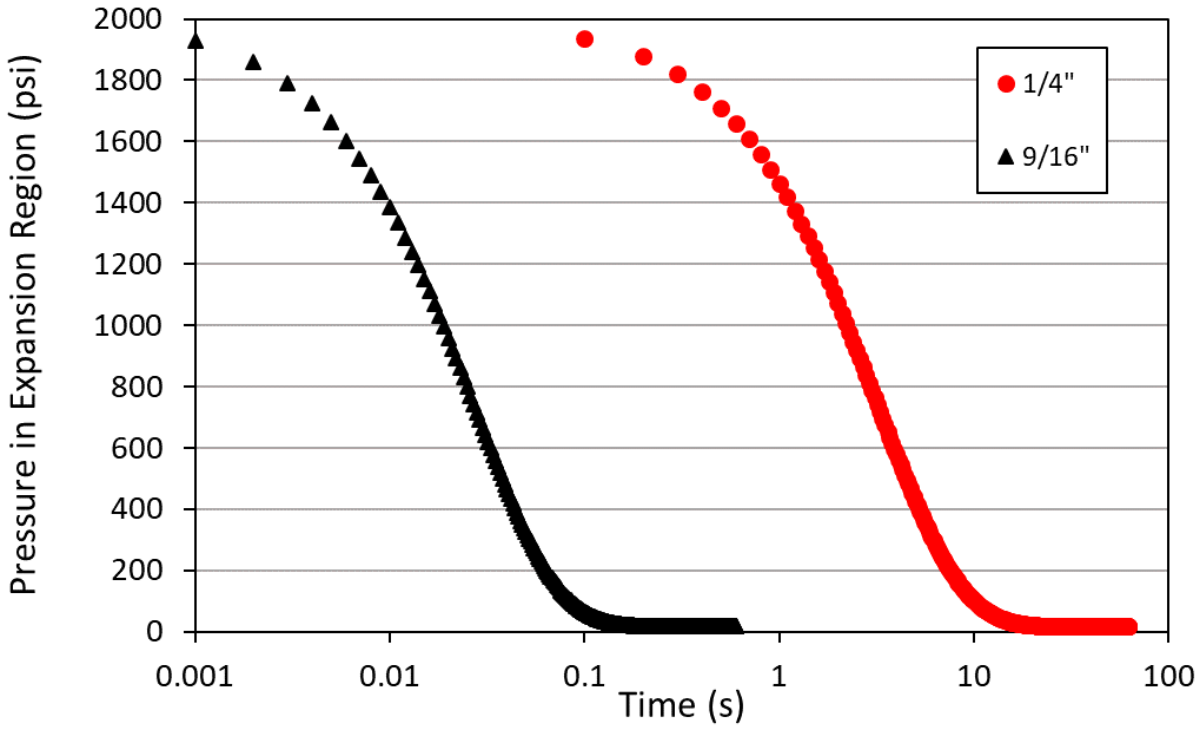

Figure 11. A graph showing the predicted venting times of the expansion chamber with both the old diameter venting lines (red circles) and the new larger diameter venting lines (black triangles).

The new cell design includes sacrificial copper sleeves and nozzles. These copper pieces can be easily removed and cleaned of metal deposits or replaced entirely if metal buildup is substantial. The designs of these sacrificial liners are shown below in Figure 12. The previous expansion cell required periodic reaming to clear particle buildup in the barrel of the shock tube. The new copper nozzles allow quick replacement if buildup is a concern downstream of particle seeding. The nozzle is mounted as near to the particle loading ports as possible, to minimize any particle build-up on the Monel K500 portions of the shock tube. These nozzles are machined in house in bulk and can be replaced as needed. The other two design aspects are two copper sleeves; one for the main chamber and the others extending in the window arms. These two fitted sleeves are manufactured from commercially available pipe sizes and only require in-house drilling of holes for vent lines and window arms. By initially inserting the window arm sleeves and manufacturing the chamber sleeve to have window openings slightly undersized, the entire copper liner will maintain its position without any adhesives or connectors. Due to the thermal resistance of copper [7], this liner provides mitigation for material build-up in the expansion chamber and eliminates any concerns of incomplete cleaning prior to operation. This also eliminates the need for volatile organic compounds (ethanol, lubricants, etc.) that have been used in the past for cleaning. Insufficient evaporation and pump down of these cleaning materials was also considered a potential failure mechanism. Any metal deposits formed on these liners can be machined off, or the liners can be replaced entirely if degradation is significant.

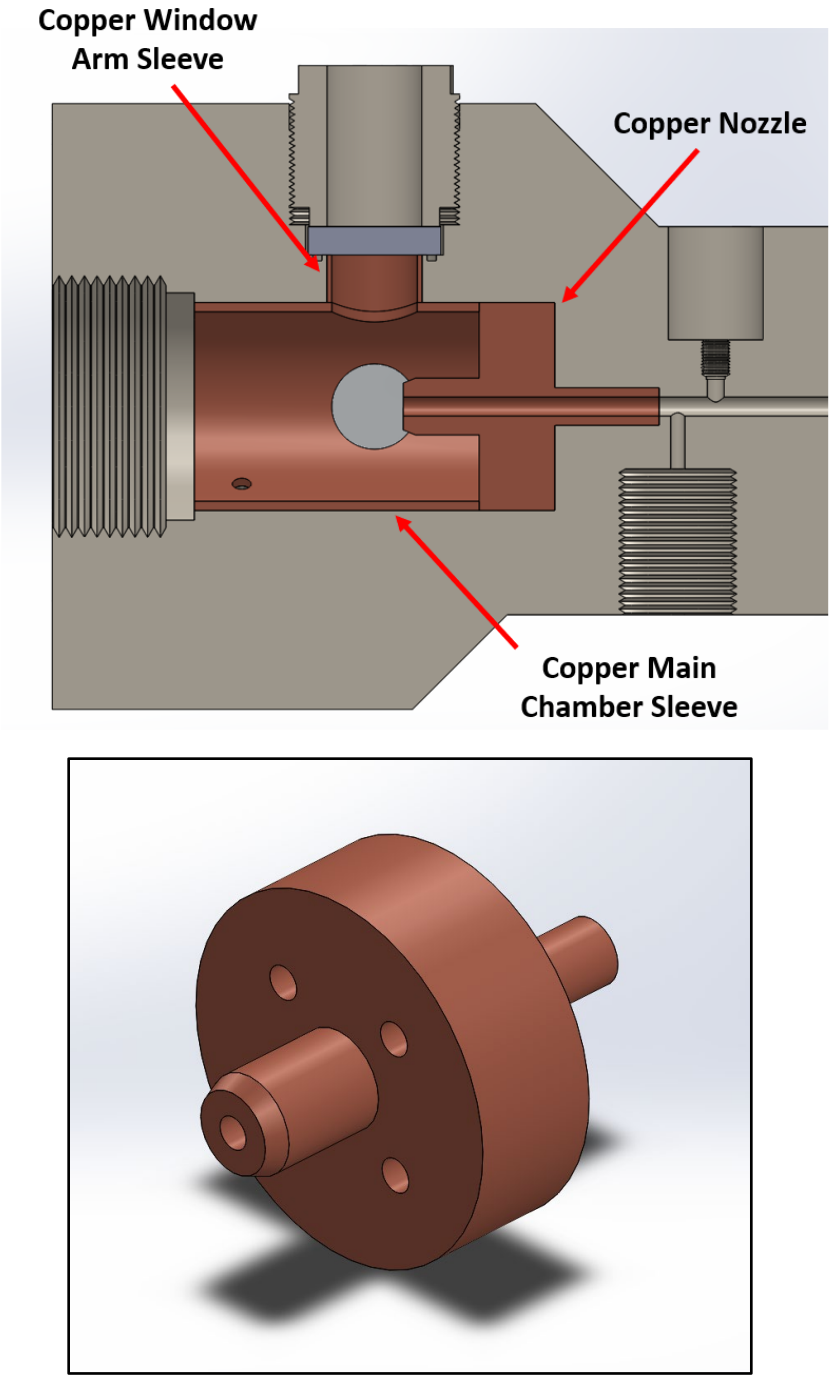

Figure 12. A model of the three sacrificial copper fittings in the new expansion chamber design. The lower image shows a closeup of the copper nozzle insert.

3. Performance and Results

Prior to final machining of the new expansion region, the factor of safety of the new chamber was estimated with a finite element model (FEM) [9][10]. This was performed assuming a worst-case scenario at an operating pressure of 4000 psi, which simulates the dynamic pressure experienced by the expansion region following a shock wave. For this simulation, thermal effects were predicted to have a marginal contribution.

The peak stress observed from FEM was 8.5 ksi, which occurred near the interior corners of the window arms, shown in Figure 13 below. The scaling used in Figure 13 is arbitrary to show relative stress at a given location. A conservative estimate of the allowable pressure of the expansion region was found to be 90 ksi, giving a factor of safety greater than 10. The allowable pressure represents the maximum amount of pressure that can be applied to the interior of the expansion region before failure. The fatigue limit of the new chamber design was calculated to be 30 ksi. The fatigue limit represents the maximum allowable operating pressure before fatigue results in the expansion chamber due to pressure cycling, which occurs during normal operation of the particle shock tube.

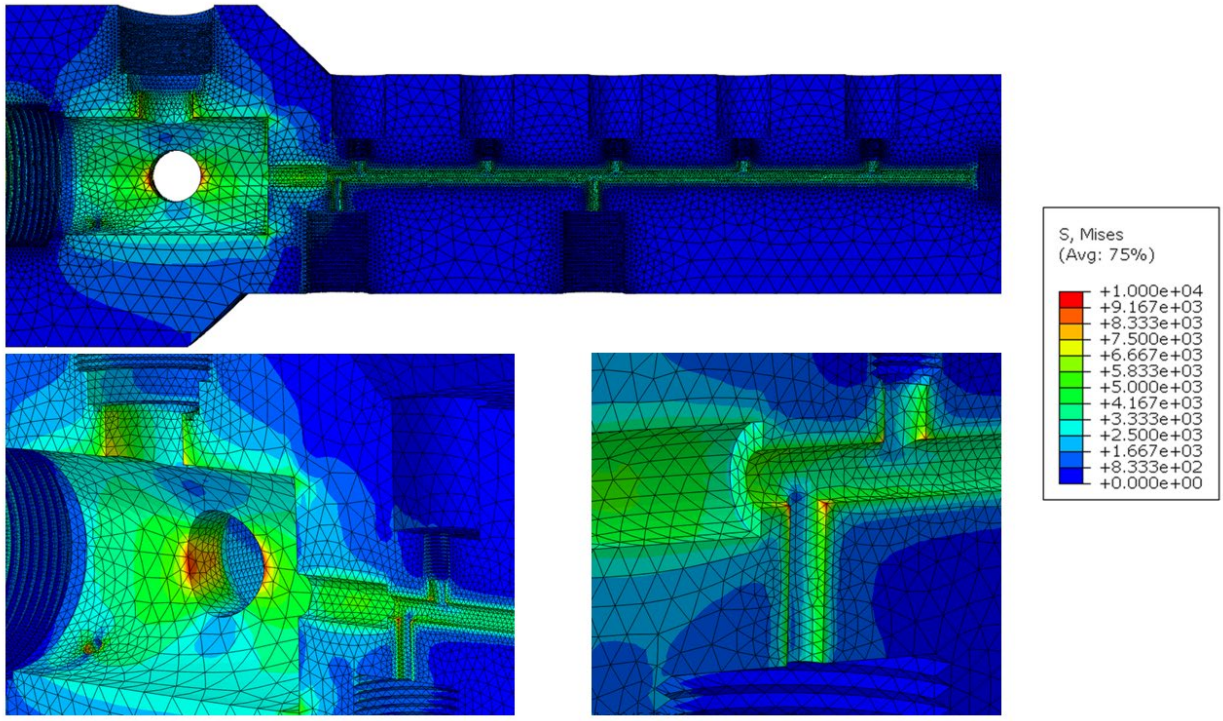

Figure 13. Images from the FEM analysis predictions of the new expansion section.

After final machining, the Monel K500 expansion section was then hydrotested up to 6000 psi. For this test, the existing antechamber was attached to the test section and aluminum disks were mounted in the window arms. The sapphire windows utilized in the PST have been failure tested to 10.7 ksi and represent the limiting component in high pressure work in the new PST design. Overall, the hydrotesting to 6000 psi represents a safety factor of three over the maximum allowable static operating pressure of the expansion region.

Characterization of the redesigned PST was initially performed with nitrogen in the driven section, to reduce the chances of chamber damage. A pressure trace resulting from a driven section fill pressure of

700 psi (nitrogen) and a helium burst pressure of 30 ksi is presented in Figure 14. This pressure trace was measured with an Endevco model 8511A-10K piezo-resistive pressure transducer mounted in the expansion region at the same impact plane position as the metal target samples. This pressure trace shows several reflections within the chamber, seen in the oscillating peaks after the initial pressure rise. The shock speed was determined to be 171 m/s.

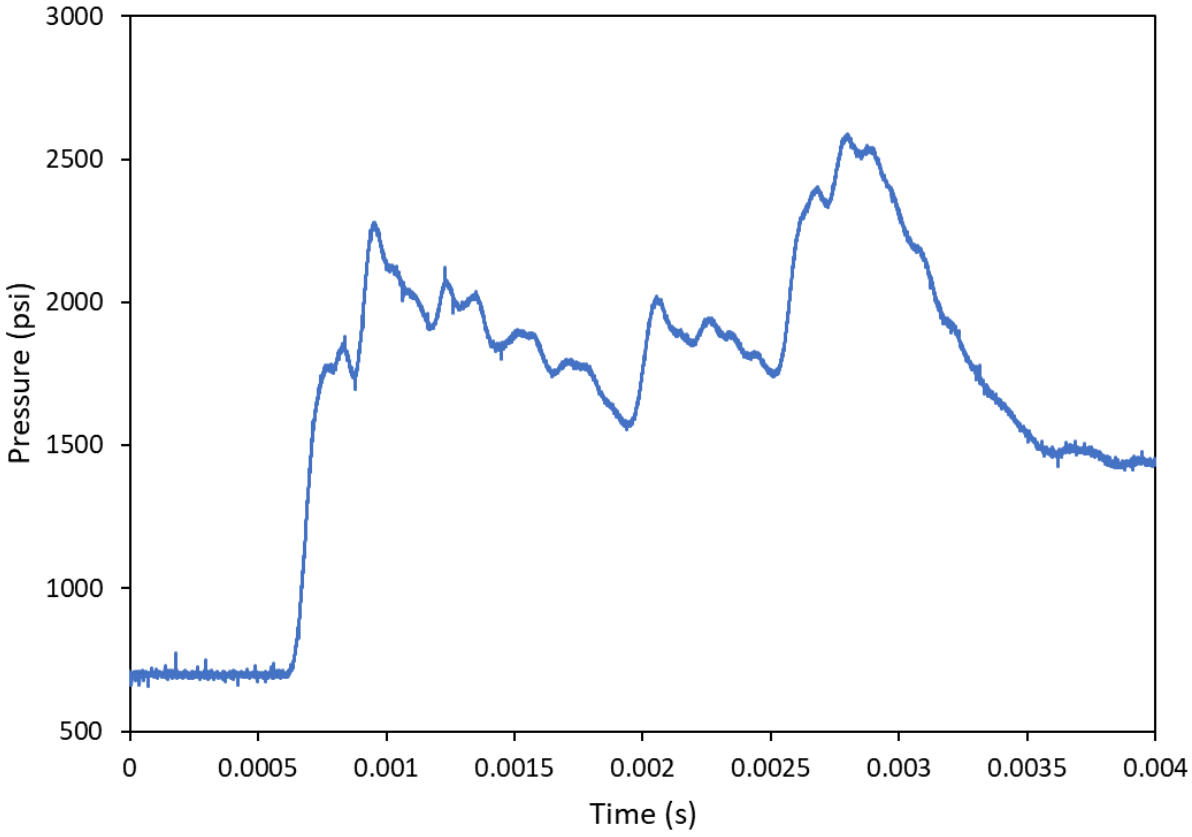

Figure 14. Pressure trace from the new PST expansion cell. The driven section pressure was 700 psi and the driver region burst pressure was 30 ksi. Several shock reflections are observed after the initial shock wave impact.

The transformation of the pressure trace data from time to frequency space is shown in Figure 15. This frequency data shows a sharp peak at 1812 Hz. This frequency corresponds to the travel time of the primary shock wave reflecting within the expansion cell. It should be noted that for these pressure measurements, the antechamber expansion region was not attached to the expansion cell. This results in significantly more reflected shocks than a nominal experimental run in the PST. It is believed that the oscillating peaks seen in Figure 14 are the result of these shock reflections in the smaller volume of the capped expansion cell. These shock reflections increase in magnitude with an increase in the ratio of driver burst pressure to expansion region pressure and were observed at burst pressures up to 47 ksi and expansion region pressures of 2000 psi.

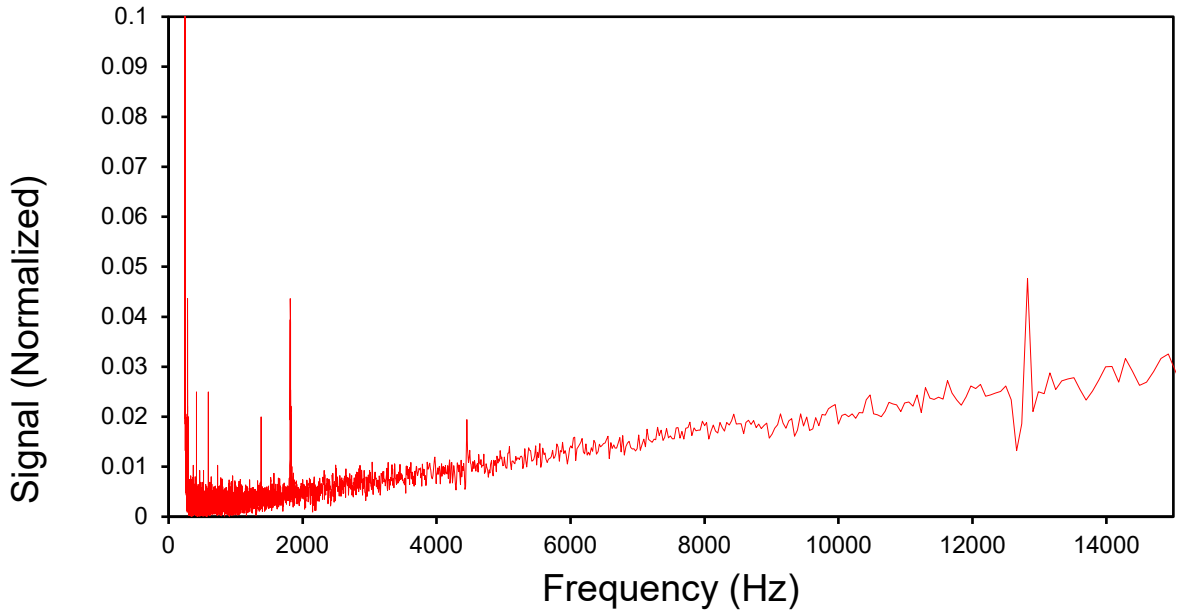

Figure 15. The pressure trace shown in Figure 14 converted to frequency space. A clear peak is visible at 1812 Hz.

The speed of the shock (171 m/s) matches the shock speed determined in the previous shock tube configuration for the same conditions. The change in the position of the particle seeding port, closer to the expansion region, provides higher dynamic pressures of oxygen at the target at the time of particle impacts, due to their earlier arrival time. This higher oxygen pressure is more representative of the conditions of interest for staged combustion engines. Increases to the static oxygen fill pressure of the driven section are planned but are not addressed in this work.

4. Conclusions

The Particle Shock Tube experimental facility located at the Aerospace Corporation has recently undergone rebuilding and improvements. These changes have resulted in both a safer experimental testing apparatus as well as potentially allowing higher operating pressures in the future, which is of for materials testing at conditions relevant to staged-combustion rocket engines. These facility modifications include a thicker driver section wall, an expendable copper liner, weldless window arms, and a hardened Monel K500 chamber. The new configuration has successfully passed hydrotesting to 6000 psi, and nitrogen/helium shocks have been characterized in the new driven section.

5. Acronyms

AM	Additively Manufactured
EDM	Electrical Discharge Machining
EDS	Energy Dispersive X-ray Spectroscopy
FEM	Finite Element Model
PST	Particle Shock Tube

6. References

[1] Herzo, D., Seyda, V., Wycisk, E., and Emmelmann, C., "Additive Manufacturing of Metals", *Acta Materialia* **117**, 371-392 (2016).

[2] Lam, K. Y., Crofton, M. W., Arnold, D. G., Morehart, J. H., "Particle-Impact Ignition of Metals in High-Pressure, Oxygen-Rich Environments", *AIAA Propulsion and Energy Forum*, Indianapolis, IN (2019).

[3] "Handling Precautions for Viton and Related Chemicals", Technical Document from Chemours

[4] D'Alfonso, A. J., Freitag, B., Klenov, D., Allen, L. J., "Atomic-resolution Chemical Mapping using Energy-Dispersive X-ray Spectroscopy", *Phys Rev B* **81**, 100101 (2010).

[5] Allen, L. J., D'Alfonso, A. J., Freitag, B., Klenov, D. O., "Chemical Mapping at Atomic Resolution using Energy-dispersive X-ray Spectroscopy", *MRS Bulletin* **37,** 47 (2012).

[6] "Safety Standard for Oxygen and Oxygen Systems", *Office of Safety and Mission Assurance,* NASA, Washington D. C. (1996).

[7] Clark, A. F., Hust, J. G., "A Review of the Compatibility of Structural Materials with Oxygen", *AIAA J* **12**, 441-454 (1974).

[8] Moore, J. H., Davis, C. C., Coplan, M. A., "Building Scientific Apparatus", *Cambridge University Press,* Fourth Edition, Chapter 3 (2009).

[9] Zienkiewicz, O. C., "The Finite Element Method", *McGraw-Hill*, 3rd Edition, *London* (1977).

[10] Reddy, J. N., "An Introduction to the Finite Element Method", *McGraw-Hill,* 2nd Edition, *New York* (1993).

Technical Reports Addendum Asset Summary #20201124080909320009

Report Name: Redesign of the Particle-Impact Shock Tube and Preliminary Data Analysis
Aerospace Report Number: TOR-2020-01948

First Aerospace Author / PI: Dr. Joshua D Winner
Created By: Dr. Joshua D Winner

NON Aerospace MTE: *No assets reported.*

AEP680 ENDEVCO 8511A-5K Usage Dates: 02/10/2020 - 03/16/2020

Calibration Date	Calibration Due Date	Certificate Number	Certificate Notes
06/20/2019	07/19/2020	3F8F8199-9D2A-45C6-BF51-5B34C43D814A	TMT-NORMAL

AEROSPACE REPORT NO.
TOR-2020-01948

Redesign of the Particle-Impact Shock Tube and Preliminary Data Analysis

Approved Electronically by:

Thomas J. Curtiss, DIRECTOR - DEPARTMENT
SPACE MATERIALS LABORATORY
PHYSICAL SCIENCES LABORATORIES
ENGINEERING & TECHNOLOGY GROUP

Cognizant Program Manager Approval:

John C. Di Pol, SYSTEMS DIRECTOR
DEVELOPMENTAL PROTOTYPES AND PROJECTS
ADVANCED DEVELOPMENT & PLANNING DIVISION
DEFENSE SYSTEMS GROUP

Aerospace Corporate Officer Approval:

Malina M. Hills, SENIOR VP SPACE SYSTEMS GROUP
OFFICE OF EVP

Content Concurrence Provided Electronically by:

Joshua D. Winner, SENIOR MEMBER OF TECHNICAL STAFF
CHEMICAL PROPULSION & ENVIRONMENTAL SCI
PROPULSION SCIENCE DEPT
ENGINEERING & TECHNOLOGY GROUP

SY0653

AEROSPACE REPORT NO.
TOR-2020-01948

Redesign of the Particle-Impact Shock Tube and Preliminary Data Analysis

Technical Peer Review Performed by:

Andrew C. Cortopassi, MGR-LABORATORY
PROPULSION SCIENCE DEPT
SPACE MATERIALS LABORATORY
ENGINEERING & TECHNOLOGY GROUP

SY0653